Non-Annealed Graphene Paper as a Binder-Free Anode for Lithium-Ion Batteries

ARTICLE *in* THE JOURNAL OF PHYSICAL CHEMISTRY C · JULY 2010

Impact Factor: 4.77 · DOI: 10.1021/jp103704y

Non-Annealed Graphene Paper as a Binder-Free Anode for Lithium-Ion Batteries

Ali Abouimrane,[†,§] Owen C. Compton,[‡,§] Khalil Amine,*[,†] and SonBinh T. Nguyen*[,‡]

Materials Sciences and Engineering Division, Argonne National Laboratory, 9700 South Cass Avenue, Argonne, Illinois 60439, and Department of Chemistry and The International Institute for Nanotechnology, Northwestern University, 2145 Sheridan Road, Evanston, Illinois 60208-3113

Received: April 25, 2010

Non-annealed graphene paper, prepared via reduction of prefabricated graphene oxide paper with hydrazine hydrate, was employed as the sole component of a binder-free lithium-ion battery anode, circumventing the polymer binders and other additives required for the fabrication of conventional electrodes. The binder-free anode fabricated from this non-annealed paper possessed excellent cyclability, while exhibiting a voltage versus capacity profile similar to that of a polymer-bound graphene powder anode. Kinetic barriers may exist for Li ion diffusion through the layered paper structure as decreasing the current rate from 50 to 10 $mA \cdot g^{-1}$ increased the reversible capacity by over 150%.

Introduction

In 1983, research and development on lithium batteries achieved a breakthrough when a pure lithium metal anode was substituted by a graphitic carbon material in which lithium was reversibly intercalated and deintercalated.[1] The lamellar structure of graphite discouraged the formation of lithium dendrites and improved thermal stability, both major problems associated with lithium metal, allowing the lithium-ion battery (LIB) to be successfully commercialized as a secondary, rechargeable battery in 1991.[2] In graphitic carbons, lithium can form intercalation compounds with a stoichiometry of LiC_6, giving LIBs a maximum theoretical capacity of only 372 $mAh \cdot g^{-1}$. Ongoing research efforts have focused on utilizing various carbonaceous nanomaterials to improve this moderate battery capacity as well as cycle life and charge−discharge rates.

Given the excellent combination of structural and electronic properties of single-walled carbon nanotubes (SWNTs),[3] they have been investigated as alternatives to graphite for LIB anodes, exhibiting a high specific capacity (~500 $mAh \cdot g^{-1}$) and good cyclability.[4] Because SWNTs can be assembled into paper-like sheets or mats, they can function as the sole component of an LIB anode, in contrast to conventional graphite-based anodes that consist of mixtures of the active Li-bearing graphite, electrical conductor, polymer binder, and solvent. Although this binder-free anode affords increased capacity, many barriers remain that impede the commercial use of SWNTs as anodes for LIBs: (1) SWNTs tend to clump together during processing, (2) achieving bulk quantities of SWNTs with narrowly dispersed diameters and chiral angles is difficult, and (3) production costs are high.

Graphene, essentially an "unrolled", two-dimensional SWNT, has recently attracted tremendous attention from both experimental and theoretical scientific communities.[5,6] It has been investigated for a variety of applications, including microelectronic devices, batteries, supercapacitors, sensors, biomedicines, and mechanical resonators.[7] With respect to LIBs, a graphene-based anode would circumvent the barriers (as outlined above) that currently impede application of SWNT-based anodes. Additionally, the high surface area (~2600 $m^2\ g^{-1}$ per sheet in theory)[8] and excellent electronic properties (thermal conductivity is 3000 $W\ m^{-1}\ K^{-1}$)[9] of graphene suggest that it may be incorporated as an electrode component into a stable, high-capacity LIB. Indeed, a 2008 report by Yoo et al.[10] has shown that an LIB anode made from graphene powder and poly(tetrafluoroethylene) binder can reach a reversible capacity of 540 $mA \cdot g^{-1}$ in the first cycle; however, this capacity drops to 290 $mAh \cdot g^{-1}$ after 20 cycles. Moderate improvements in both the capacity and the cyclability of polymer-bound graphene powder LIB anodes have since been reported.[11,12]

Here, we present non-annealed graphene paper, prepared via hydrazine reduction of prefabricated graphene oxide paper,[13] as a binder-free alternative *anode* to recently reported graphene-based electrodes that are fabricated from a mixture of polymer binder and active material.[10−12] Our graphene paper anode exhibits a charge−discharge profile that closely resembles those reported for polymer-bound graphene-based anodes[10−12] while maintaining excellent cyclability over 70 charge−discharge cycles. Significant increases in the reversible capacity (from 84 to 214 $mAh \cdot g^{-1}$) were observed when the current rate was decreased from 50 to 10 $mA \cdot g^{-1}$, suggesting possible kinetic barriers to Li ion diffusion as a result of the layered structure of the graphene paper anode.

Experimental Methods

Materials. All chemicals were used as received from commercial sources unless otherwise noted. SP-1 graphite powder was purchased from Bay Carbon (Bay City, MI). Hydrazine monohydrate (98%, 64−65 wt % N_2H_4) was obtained from Sigma-Aldrich (St. Louis, MO) and stored under nitrogen to discourage oxidation. Ultrapure deionized water (resistivity >18 $M \cdot \Omega$) was obtained from a Millipore Mili-Q Biocel system.

Graphene Oxide Synthesis. Graphite oxide was prepared by oxidizing SP-1 graphite powder (2 g) using a modified Hummers method.[14,15] The product (~2.7 g of graphite oxide) was purified by five cycles of centrifugation (Eppendorf model 5804 R, 30 min at 8000 rpm) and washing with ultrapure deionized water (30 mL), followed by dialysis (Spectra/Por

* To whom correspondence should be addressed. E-mail: amine@anl.gov (K.A.), stn@northwestern.edu (S.T.N.).
† Argonne National Laboratory.
‡ Northwestern University.
§ A.A. and O.C.C. contributed equally to this work.

10.1021/jp103704y
Published on Web 06/30/2010

Membrane, 6−8 kD MWCO) in ultrapure deionized water (4 × 2 L over a period of 2 days). After this process, the suspended materials in the dialysis bag were centrifuged down to a pellet and the supernatant was decanted away. The remaining pellet was resuspended in ultrapure deionized water (100 mL to make as suspension of ∼5 mg mL^{-1}), combined with aqueous NaOH (1 mL of a 0.1 M solution) to promote exfoliation,[16] and thoroughly dispersed in water by immersion in a bath sonicator (Fisher Scientific FS60) for 30 min.

Further purification to remove unexfoliated graphite oxide was then performed by subjecting the aforementioned basified graphene oxide dispersion to five additional cycles of centrifugation (8000 rpm for 30 min) and washing with ultrapure deionized water (30 mL), this time with the supernatant (containing the exfoliated graphene oxide) retained and the precipitate disposed. The remaining suspension was then dialyzed (Spectra/Por Membrane, 6−8 kD MWCO) in ultrapure deionized water (4 × 2 L over a period of 2 days) to remove any remaining sodium ions. The final dispersions were diluted with ultrapure deionized water to ∼1 mg mL^{-1} before further processing.

Fabrication of Graphene Oxide Paper. Graphene oxide paper, the precursor to graphene paper, was prepared according to previously reported protocols.[17] A dilute aqueous graphene oxide dispersion (∼1 mg mL^{-1}, 30 mL) was filtered through a Whatman Anodisc membrane (0.2 μm pore size, 47 mm diameter) under vacuum assistance using a Kontes Ultraware microfiltration apparatus with a fritted glass support base. The assembled paper was left in the filtration apparatus and immediately carried through hydrazine reduction.

Reduction of Graphene Oxide Paper to Graphene Paper. Reductive treatment was initiated immediately after graphene oxide paper fabrication. Once all the solvent had passed through the membrane, the paper appeared moist and black, a state we have previously referred to as "wet".[13] Allowing the graphene oxide paper to dry for as little as 1 h on the membrane would generate undesirable gaps between the paper edge and filter reservoir, where solution could pass through, negating complete reaction with the layered paper structure. As such, while still in the Kontes filtration apparatus, "wet" graphene oxide paper was reduced by filtering aqueous hydrazine monohydrate (50 mL of a 2.0 M solution) through the membrane-supported paper at 90 °C for ∼5 h under assistance from house vacuum.[13] The temperature was maintained during the filtration process by fitting the filter reservoir with a heating mantle jacket. Ultrapure deionized water (50 mL) was then filtered through the resulting graphene paper for 15 h under vacuum assistance to wash away residual hydrazine. After washing, the paper was removed from the filtration apparatus and air-dried prior to electronic and physical characterization.

Preparation of Graphene Powder. Graphene powder was prepared according to the literature[8] by stirring a dilute aqueous graphene oxide dispersion (∼1 mg mL^{-1}, 30 mL) and hydrazine monohydrate (10 molar excess) at 90 °C for ∼5 h. Graphene aggregates, formed during the reduction process, were filtered and washed with ultrapure deionized water (3 × 50 mL) to remove residual hydrazine. After washing, the graphene powder was air-dried prior to electronic and physical characterization.

Electronic and Physical Characterization. Charge−discharge profiles and cycle performance data for graphene paper and graphene powder electrodes were assembled in a CR 2032-type coin cell configuration and collected using a Maccor battery cycler (Maccor, Inc., Tulsa, OK). Lithium metal foil served as the counter electrode and the electrolyte consisted of a 3:7 w/w mixture of ethylene carbonate and ethyl methyl carbonate, with lithium ions present in the form of $LiPF_6$ (1.2 M). All samples were heated at 75 °C for 3 h to remove residual moisture before being transferred to a He-filled glovebox. For evaluation of the graphene paper electrode, a small piece of graphene paper was used exclusively, whereas the graphene powder electrode was prepared by mixing the powder with poly(vinylidene fluoride) at a mass ratio of 8:2. Both types of cells were charged and discharged under the same current density.

Instrumentation. The size of graphitic regions in the graphene paper was evaluated using an Acton TriVista Confocal Raman System (Princeton Instruments, Acton, MA) with laser excitation (λ = 514.5 nm). The morphology of the paper was visualized via scanning electron microscopy (SEM) using a Nova NanoSEM 600 (FEI Co., Hillsboro, OR) microscope. Spacing between adjacent graphene layers was determined using X-ray diffraction (XRD) with a Rigaku XDS 2000 diffractometer (Rigaku America Corp., The Woodlands, TX) using nickel-filtered Cu Kα radiation (λ = 1.5418 Å). X-ray photoelectron spectroscopy (XPS) was performed with an Omicron ESCA Probe (Omicron Nanotechnology GmbH, Taunusstein, Germany) using Al Kα radiation ($h\nu$ = 1486.6 eV). A Shirley background was removed from the spectra before deconvolution.

Results and Discussion

It is well-known that treatment of graphene oxide, in any morphological form, with hydrazine at elevated temperatures affords graphene.[8,18] As such, we have subjected graphene oxide paper and an aqueous graphene oxide dispersion to similar reductive conditions (excess hydrazine monohydrate at 90 °C for 5 h) to afford graphene paper and graphene powder, respectively. Both forms of graphene exhibited similar C 1s XPS spectra (Figure 1A,B) with significant deoxygenation in comparison with nonreduced graphene oxide paper (Figure S1 in the Supporting Information). Similar to previous reports,[8,19] the XPS spectra of both of our graphene materials comprised primarily sp^2 C 1s signals, with only small contributions from epoxy, hydroxyl, carbonyl, and carboxyl groups. The I_D/I_G ratios seen in the Raman spectra of our graphene paper and powder (Figure 1C,D) verified that significant graphitic regions existed within these reduced materials.[20] From the Tuinstra−Koenig relation, the 0.9 intensity ratio of the D (∼1345 cm^{-1}) and G (∼1570 cm^{-1}) bands in the spectrum of our graphene paper (Figure 1C) corresponded to ordered graphitic regions of ∼5 nm within the paper structure. Such regions could each accommodate ∼450 C_6 rings, which, in turn, could bind ∼75 Li atoms in the fully charged state, assuming a LiC_6 stoichiometry. The larger I_D/I_G ratio of 1.4 in the spectrum for graphene powder (Figure 1D) indicated a more disordered graphene structure with smaller sp^2 domains.

SEM imaging revealed a smooth undulating morphology on the graphene paper surface (Figure 2A), with a wavy, layered structure along the fracture edge, not unlike that previously observed for graphene oxide paper.[17] Minor local structural heterogeneities (Figure 2B), observable as void spaces along the fracture edge of the paper, were likely a result of N_2 and H_2O evolution during hydrazine reduction[13] and produced variances in thickness from 7 to 10 μm. Such minor variances were also evident in the fine structure of the paper, as seen in its broader XRD pattern compared to graphene oxide paper (Figure 3). A broad peak corresponding to an average intersheet spacing of 3.70 Å was present for our graphene paper, comparable to that of graphite powder (3.34 Å) and significantly shifted from that of graphene oxide paper (8.75 Å). Although

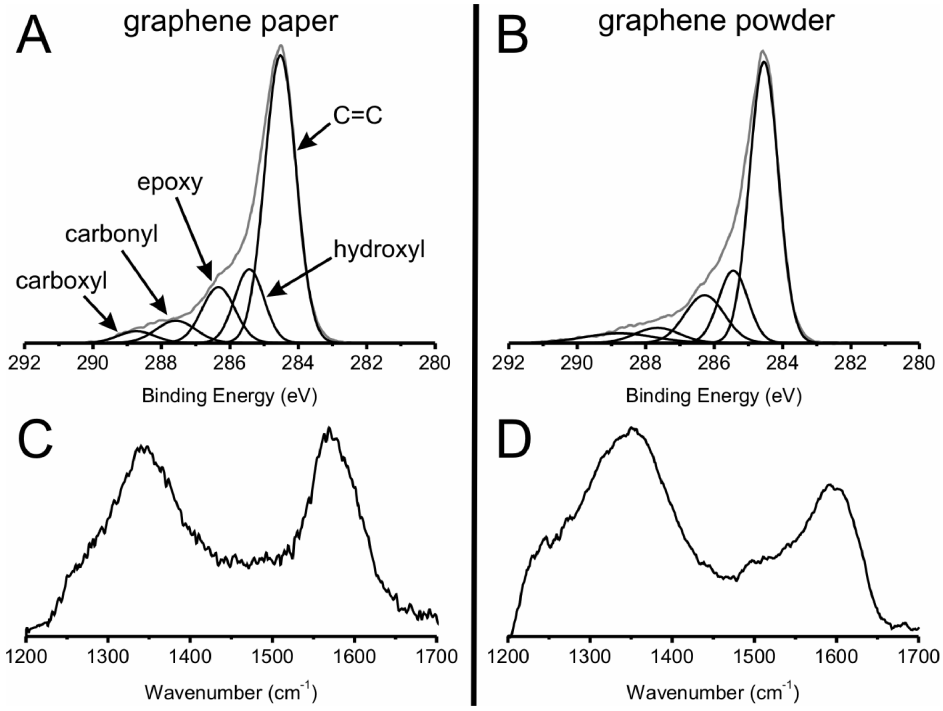

Figure 1. (A, B) XPS spectra of the C 1s regions of graphene paper and graphene powder, demonstrating the relatively low levels of oxygen-containing functional groups. (C, D) Raman spectra of graphene paper and graphene powder, illustrating the differences in the intensities of the D (~1345 cm^{-1}) and G (~1570 cm^{-1}) bands of the anode materials.

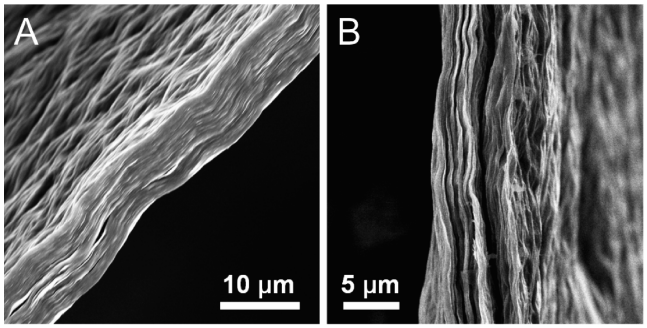

Figure 2. SEM images of graphene paper showing the (A) undulating paper surface and (B) local heterogeneities along a fractured edge.

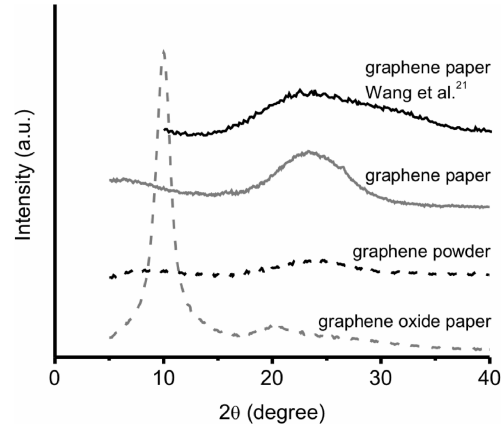

Figure 3. XRD patterns contrasting the higher level of order in our anodic graphene paper against the lower-ordered cathodic graphene paper used by Wang et al. The pattern for graphene oxide paper is included to illustrate the shift in paper spacing after reduction. For comparison, the pattern for graphene powder is also presented.

the broadness of this peak suggested minor variances in spacing between layers within the graphene paper structure, this should not be misconstrued as a result of random packing within the graphene paper structure. Indeed, the XRD pattern (Figure 3) for our paper was sharper and more intense than data reported by Wang et al.[21] for a graphene paper electrode fabricated from an aqueous dispersion of graphene sheets (see below), indicating a more well-ordered structure.

The galvanostatic charge and discharge curves for both of our graphene-based electrodes (Figure 4) showed an irreversible charge−discharge profile (capacity ratios are 3.2 and 2.4 for the graphene paper and graphene powder electrodes, respectively) during the first cycle. This behavior is often seen in graphitic LIB electrode materials and could be attributed to either residual oxygen-containing functional groups in the materials, seen in the XPS spectra (Figure 1A,B), or the formation of a solid−electrolyte interface (SEI) layer on the surface of the electrodes. However, the charge−discharge profiles for our graphene-based electrodes are more similar to those observed for disordered carbon and are distinctly different that of graphite powder,[10] which possesses crystalline layered graphene sheets. The charge−discharge profile for graphite powder exhibits a distinguishable voltage plateau during charging at ~0.15 V versus Li/Li^+.[10] The absence of this plateau in the charge−discharge profile of our graphene electrodes mirrors that in disordered carbon, where noncrystalline stacking of the nanosheets generates a variety of nonequivalent lithium ion sites.[22] This similarity suggests that the graphene sheets in our electrodes are largely disordered, as confirmed by the presence of a strong D band in both Raman spectra (Figure 1C,D).

Similar to most graphite- and graphene-based LIB electrodes, our non-annealed, binder-free graphene paper electrode exhibited a poor charge−discharge Coulombic efficiency (i.e., the % ratio of charge to discharge capacity) during the first cycle (~27%) under a current rate of 50 $mA \cdot g^{-1}$ (Figures 4 and 5). However, the cyclic performance and Coulombic efficiency of the Li/graphene paper half-cell was significantly enhanced after a few cycles (Figure 5). Indeed, after only 10 cycles at that same

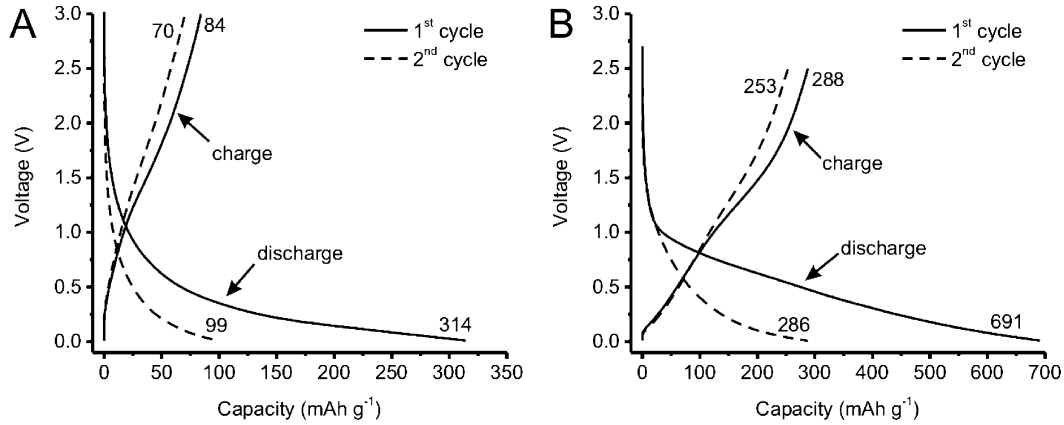

Figure 4. Charge−discharge profiles of a Li/graphene half-cell at a current rate of 50 mAh·g^{-1}, where the graphene component is either (A) graphene paper or (B) graphene powder.

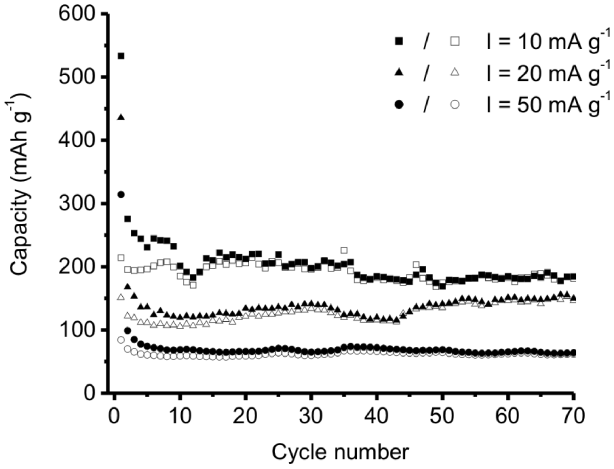

Figure 5. Cycle performance of a Li/graphene paper half-cell at three different current densities. Charge and discharge capacities under each current density are represented by open and solid shapes, respectively.

current rate, the charge−discharge Coulombic efficiency reached 86% with further improvement to 98% after 70 cycles. This good cycling performance could be attributed the formation of a stable SEI layer.[4]

Under a 50 mA·g^{-1} current rate, our graphene paper and PVDF-graphene powder anodes exhibited initial reversible capacities of 84 and 288 mAh·g^{-1}, respectively (Figure 4). The larger reversible capacity for the latter anode may be attributed to the more disordered packing of the graphene sheets (Figure 3), which is conducive to anisotropic Li diffusion. Supporting this hypothesis is the observation that our graphene paper anode exhibited increasing initial reversible capacities of 84, 151, and 214 mAh·g^{-1} under, respectively, decreasing current rates of 50, 20, and 10 mA·g^{-1} (Figure 5). Presumably, the well-ordered structure of the graphene paper would present a kinetic barrier for the diffusion of Li ions out of the anode during delithiation. We note that an increase of over 150% in reversible capacity when the current rate is lowered from 50 to 10 mA·g^{-1} is especially remarkable considering that anodes made from polymer-bound, disordered graphene sheets exhibited a variance of only 1% in initial reversible capacity when the current density was lowered from 100 to 20 mA·g^{-1}.[12]

Both of our electrodes exhibited galvanostatic charge−discharge curves that were similar to those observed for polymer-bound graphene anodes[10−12] and did not feature an initial plateau near 2.2 V during discharge, as observed for a similar non-annealed graphene paper prepared Wang et al.[21] We suspect that the mineral oil surfactant that these authors used in the preparation of their graphene paper[23] may be responsible for this observed cathodic behavior. Indeed, after annealing at 800 °C, where mineral oil would have surely evaporated or decomposed, Wang et al. did not observe such a plateau and this annealed graphene paper exhibited anodic behavior. The presence of the mineral oil surfactant may also explain the low level of order in the graphene paper used by Wang et al., as evidenced by its broad XRD peak in comparison to that of our materials (Figure 3). Because our graphene paper was prepared via hydrazine reduction of prefabricated graphene oxide paper, *anodic behavior can be directly achieved without annealing*. In conjunction with the good discharge capacity and excellent cyclability (see above), our graphene paper holds promise as a single-component anode for use in high-capacity LIBs.

Conclusions

In summary, we have demonstrated that non-annealed graphene paper, produced via hydrazine reduction of prefabricated graphene oxide paper, is suitable for use as a binder-free anode in *secondary*, *rechargeable* LIBs with both good capacity and excellent cyclability. Because our graphene paper serves as a single-component anode, its use as an LIB electrode could significantly improve battery capacity/weight ratio in comparison to multicomponent electrodes that are fabricated from a mixture of polymer binder and active material. In addition to simplifying anode fabrication, by circumventing processing steps, such as polymer mixing and high-temperature treatment, the use of binder-free graphene anodes would also reduce manufacturing costs. Given its ease of access,[13] excellent mechanical properties,[24] light weight, and low cost, our graphene paper is a highly promising candidate to compete against SWNT-based materials as an anode for incorporation in high-capacity LIBs. Efforts to improve both its electronic conductivity and its reversible charge capacity under high current rates are underway.

Acknowledgment. This work was supported by the U.S. Department of Energy (FreedomCar, Vehicle Technology Office), the NSF (Award No. DMR-0520513 through the Materials Research Science and Engineering Center at Northwestern University), and ARO (Award No. W991NF-09-1-0541). O.C.C. is an NSF-ACC fellow (Award No. CHE-0936924). We thank Prof. Mark Ratner for helpful discussions. The authors also thank UChicago Argonne, LLC, Operator of Argonne National Laboratory ("Argonne"). Argonne, a U.S. Department of Energy Office of Science laboratory, is operated under Contract No. DE-AC02-06CH11357.

Supporting Information Available: Additional materials characterization (XPS, TGA, and FT-IR data) and electrochemical measurements. This material is available free of charge via the Internet at http://pubs.acs.org.

References and Notes

(1) Yazami, R.; Touzain, P. *J. Power Sources* **1983**, *9*, 365–371.
(2) Nagaura, K.; Tozawa, K. *Prog. Batteries Sol. Cells.* **1990**, *9*, 209–217.
(3) Raffaelle, R. P.; Landi, B. J.; Harris, J. D.; Bailey, S. G.; Hepp, A. F. *Mater. Sci. Eng., B* **2005**, *116*, 233–243.
(4) Landi, B. J.; Ganter, M. J.; Schauerman, C. M.; Cress, C. D.; Raffaelle, R. P. *J. Phys. Chem. C* **2008**, *112*, 7509–7515.
(5) Novoselov, K. S.; Geim, A. K.; Morozov, S. V.; Jiang, D.; Zhang, Y.; Dubonos, S. V.; Grigorieva, I. V.; Firsov, A. A. *Science* **2004**, *306*, 666–669.
(6) Geim, A. K.; Novoselov, K. S. *Nat. Mater.* **2007**, *6*, 183–191.
(7) Li, D.; Kaner, R. B. *Science* **2008**, *320*, 1170–1171.
(8) Stankovich, S.; Dikin, D. A.; Piner, R. D.; Kohlhaas, K. A.; Kleinhammes, A.; Jia, Y.; Wu, Y.; Nguyen, S. T.; Ruoff, R. S. *Carbon* **2007**, *45*, 1558–1565.
(9) Stankovich, S.; Dikin, D. A.; Dommett, G. H. B.; Kohlhaas, K. M.; Zimney, E. J.; Stach, E. A.; Piner, R. D.; Nguyen, S. T.; Ruoff, R. S. *Nature* **2006**, *442*, 282–286.
(10) Yoo, E.; Kim, J.; Hosono, E.; Zhou, H.-s.; Kudo, T.; Honma, I. *Nano Lett.* **2008**, *8*, 2277–2282.
(11) Wang, G.; Shen, X.; Yao, J.; Park, J. *Carbon* **2009**, *47*, 2049–2053.
(12) Guo, P.; Song, H.; Chen, X. *Electrochem. Commun.* **2009**, *11*, 1320–1324.
(13) Compton, O. C.; Dikin, D. A.; Putz, K. W.; Brinson, L. C.; Nguyen, S. T. *Adv. Mater.* **2009**, *22*, 892–896.
(14) Hummers, W. S.; Offeman, R. E. *J. Am. Chem. Soc.* **1958**, *80*, 1339.
(15) Kovtyukhova, N. I.; Ollivier, P. J.; Martin, B. R.; Mallouk, T. E.; Chizhik, S. A.; Buzaneva, E. V.; Gorchinskiy, A. D. *Chem. Mater.* **1999**, *11*, 771–778.
(16) Bissessur, R.; Scully, S. F. *Solid State Ionics* **2007**, *178*, 877–882.
(17) Dikin, D. A.; Stankovich, S.; Zimney, E. J.; Piner, R. D.; Dommett, G. H. B.; Evmenenko, G.; Nguyen, S. T.; Ruoff, R. S. *Nature* **2007**, *448*, 457–460.
(18) Becerril, H. A.; Mao, J.; Liu, Z.; Stoltenberg, R. M.; Bao, Z.; Chen, Y. *ACS Nano* **2008**, *2*, 463–470.
(19) Stankovich, S.; Piner, R. D.; Chen, X. Q.; Wu, N. Q.; Nguyen, S. T.; Ruoff, R. S. *J. Mater. Chem.* **2006**, *16*, 155–158.
(20) Tuinstra, F.; Koenig, J. L. *J. Chem. Phys.* **1970**, *53*, 1126–1130.
(21) Wang, C.; Li, D.; Too, C. O.; Wallace, G. G. *Chem. Mater.* **2009**, *21*, 2604–2606.
(22) Dahn, J. R.; Zheng, T.; Liu, Y.; Xue, J. S. *Science* **1995**, *270*, 590–593.
(23) Li, D.; Muller, M. B.; Gilje, S.; Kaner, R. B.; Wallace, G. G. *Nat. Nanotechnol.* **2008**, *3*, 101–105.
(24) Chen, H.; Muller, M. B.; Gilmore, K. J.; Wallace, G. G.; Li, D. *Adv. Mater.* **2008**, *20*, 3557–3561.

JP103704Y